Drug Design, Development and Therapy

Dovepress
open access to scientific and medical research

Open Access Full Text Article

ORIGINAL RESEARCH

Pranlukast Antagonizes CD49f and Reduces Stemness in Triple-Negative Breast Cancer Cells

This article was published in the following Dove Press journal:
Drug Design, Development and Therapy

Inés Velázquez-Quesada[1,2]
Angel J Ruiz-Moreno[1,3,4]
Diana Casique-Aguirre[1]
Charmina Aguirre-Alvarado[1]
Fabiola Cortés-Mendoza[1,5]
Marisol de la Fuente-Granada[6]
Carlos García-Pérez[7]
Sonia M Pérez-Tapia[2,8]
Aliesha González-Arenas[6]
Aldo Segura-Cabrera[9]
Marco A Velasco-Velázquez[1,10]

[1]Department of Pharmacology, School of Medicine, Universidad Nacional Autónoma de México, Mexico City, Mexico; [2]Research and Development in Bioprocess Unit, National School of Biological Sciences, Instituto Politécnico Nacional, Mexico City, Mexico; [3]Graduate Program in Biomedical Sciences, Universidad Nacional Autónoma de México, Mexico City, Mexico; [4]Department of Drug Design, Graduate School of Science and Engineering, University of Groningen (RUG), Groningen, The Netherlands; [5]Graduate Program in Biochemical Sciences, Universidad Nacional Autónoma de México, Mexico City, Mexico; [6]Department of Genomic Medicine and Environmental Toxicology, Institute for Biomedical Research, Universidad Nacional Autónoma de México, Mexico City, Mexico; [7]Center for Genomic Biotechnology, Instituto Politécnico Nacional, Reynosa, Tamaulipas, Mexico; [8]National Laboratory for Specialized Services of Investigation, Development and Innovation (I+D+i) for Pharma Chemicals and Biotechnological Products, LANSEIDI-FarBiotec-CONACyT, Mexico City, Mexico; [9]European Molecular Biology Laboratory, European Bioinformatics Institute, Hinxton, UK; [10]Peripherical Unit for Research in Translational Biomedicine, School of Medicine, Universidad Nacional Autónoma de México, Mexico City, Mexico

Correspondence: Marco A Velasco-Velázquez
School of Medicine, Universidad Nacional Autónoma de México, Circuito Interno s/n, Mexico City 04510, Mexico
Tel/Fax +52 55 5623 2282
Email marcovelasco@unam.mx

Introduction: Cancer stem cells (CSCs) drive the initiation, maintenance, and therapy response of breast tumors. CD49f is expressed in breast CSCs and functions in the maintenance of stemness. Thus, blockade of CD49f is a potential therapeutic approach for targeting breast CSCs. In the present study, we aimed to repurpose drugs as CD49f antagonists.

Materials and Methods: We performed consensus molecular docking using a subdomain of CD49f that is critical for heterodimerization and a collection of pharmochemicals clinically tested. Molecular dynamics simulations were employed to further characterize drug-target binding. Using MDA-MB-231 cells, we evaluated the effects of potential CD49f antagonists on 1) cell adhesion to laminin; 2) mammosphere formation; and 3) cell viability. We analyzed the effects of the drug with better CSC-selectivity on the activation of CD49f-downstream signaling by Western blot (WB) and co-immunoprecipitation. Expressions of the stem cell markers CD44 and SOX2 were analyzed by flow cytometry and WB, respectively. Transactivation of *SOX2* promoter was evaluated by luciferase reporter assays. Changes in the number of CSCs were assessed by limiting-dilution xenotransplantation.

Results: Pranlukast, a drug used to treat asthma, bound to CD49f in silico and inhibited the adhesion of $CD49f^{+}$ MDA-MB-231 cells to laminin, indicating that it antagonizes CD49f-containing integrins. Molecular dynamics analysis showed that pranlukast binding induces conformational changes in CD49f that affect its interaction with β1-integrin subunit and constrained the conformational dynamics of the heterodimer. Pranlukast decreased the clonogenicity of breast cancer cells on mammosphere formation assay but had no impact on the viability of bulk tumor cells. Brief exposure of MDA-MB-231 cells to pranlukast altered CD49f-dependent signaling, reducing focal adhesion kinase (FAK) and phosphatidylinositol 3-kinase (PI3K) activation. Further, pranlukast-treated cells showed decreased CD44 and SOX2 expression, *SOX2* promoter transactivation, and in vivo tumorigenicity, supporting that this drug reduces the frequency of CSC.

Conclusion: Our results support the function of pranlukast as a CD49f antagonist that reduces the CSC population in triple-negative breast cancer cells. The pharmacokinetics and toxicology of this drug have already been established, rendering a potential adjuvant therapy for breast cancer patients.

Keywords: CD49f, alpha6 integrin, breast cancer stem cells, pranlukast, drug repositioning, triple-negative breast cancer cells

Introduction

Breast cancer has the highest global incidence in women.[1] It is estimated that over 1,670,000 new breast cancer patients are diagnosed worldwide each year.[2] Despite the implementation of new targeted therapies and treatments, a high percentage of breast cancer patients still die due to tumor resistance, recurrence, and metastasis.[3] In vivo data have demonstrated that cancer stem cells (CSCs), a small subset of tumor cells,

submit your manuscript | www.dovepress.com
DovePress
http://doi.org/10.2147/DDDT.S247730

have tumor-initiating and self-renewal capacities. Accordingly, CSCs mediate the resistance to conventional therapies, metastasis, and tumor recurrence,[4] rendering them excellent targets for new anticancer treatments.

CD49f (α6 integrin; ITGA6) is a cell surface protein that forms heterodimers with β1 or β4 integrins, and the resulting complexes act as laminin-binding receptors.[5,6] Hence, CD49f-containing integrins regulate communication between cancer cells and the microenvironment. CD49f expression in human breast tumors correlates with reduced overall and recurrence-free survival rates.[7] Accordingly, its inhibition reduces the migration, invasion, and metastatic potential of breast cancer cells.[8–10]

CD49f plays a key role in stemness promotion and maintenance in breast cancer.[11,12] CD49f blockade with antibodies or CD49f knockdown decreases the in vitro clonogenicity[13] and in vivo tumorigenicity[12,14] of breast cancer cells. On the other hand, CD49f is either not expressed in non-stem breast cancer cells[15–17] or expressed but not essential for their survival.[9,10]

The key role of CD49f in stemness indicates that it can be targeted to reduce the breast CSC pool and slow up breast cancer progression. However, CD49f has not been clinically targeted, despite the fact that integrin-blocking antibodies, peptides, or small molecules are used to treat various pathologies, such as thrombosis, osteoporosis, fibrosis, and cancer.[18–21]

To repurpose drugs as CD49f antagonists, herein we performed consensus molecular docking between the β-subunit-interacting domain of CD49f and a collection of structures that are enriched in FDA-approved drugs.[22] Five in silico-selected drugs effectively blocked CD49f, inhibiting the adhesion of breast cancer cells to laminin. Pranlukast, a reported cysteinyl leukotriene receptor 1 (CysLTR) antagonist, decreased the clonogenicity of breast cancer cells by mammosphere formation assay but had no impact on the viability of bulk tumor cells. Short exposure to pranlukast reduced CD49f-downstream signaling, including Focal Adhesion Kinase (FAK) and phosphatidylinositol 3-kinase (PI3K) activation. Pranlukast-treated cells showed reduced expression of CSC markers and impaired tumorigenicity in vivo, indicating that this drug decreases the number of CSCs. Thus, pranlukast antagonizes CD49f impairing CSC-associated functions.

Materials and Methods

Molecular Docking

The primary sequences of CD49f and β1 integrin were obtained from the Uniprot database (P23229 and P05556, respectively). Human CD49f 3D model was generated by homology modeling with Modeller 9.11[23] using crystallography data from Protein Data Bank 4G1M, 4WJK, 4WK0, and 3IJE as templates. The druggability of the protein pockets was assessed using the DoGSiteScorer server tool (Hamburg University, Germany).[24] A library of 11,421 molecules (FDA-approved, withdrawn, and experimental drugs) were retrieved from the ZINC InMan subset of the ZINC[12] database (University of California, San Francisco).[22] Auto-DockTools was used to add Gasteiger charges and polar hydrogens to CD49f and the drugs. Docking was performed using AutoDock Vina 1.1.2[25] and AutoDock4[26] with a grid box that was centered on Met262 in the target model and set to 17 x 17 x 17 number of points (npts) with 0.375-Å spacing. The scores were re-evaluated with DSX_089[27] to increase the reliability and accuracy of the antagonist selection. The scores from each algorithm were used to generate Z-scores, as described.[28] The consensus score was the sum of Z-scores.

Compounds

Solutions of pranlukast hemihydrate (Sigma, catalog N° P0080), montelukast sodium hydrate (Sigma, catalog N° SML0101), imatinib mesylate (Selleckchem, catalog N° ST1571), and bromocriptine (Sigma, catalog N° B2134)—dissolved in DMSO—and zosuquidar (Selleckchem, catalog N° S1481)—dissolved in PBS—were filter-sterilized and stored at 4°C (montelukast, bromocriptine) or −20°C (pranlukast, imatinib, and zosuquidar) under light-protected conditions until use.

Cell Culture

The MDA-MB-231 cell line was purchased from ATCC and grown in Leibovitz's L-15 medium (Gibco, catalog N° 41300021), supplemented with 10% fetal bovine serum (FBS), in a carbon dioxide (CO_2)-free system. We employed cells from passage 8 to 14. Sublines that stably expressed firefly luciferase (Luc) under the *SOX2* promoter were generated by cotransfection of SOX2-Luc plasmid[29] (donated by Dr. Richard Pestell, Baruch S. Blumberg Institute, PA, USA) and pNEG-PG04. The sequence of the promoter was verified using RVprimer3. Sublines were maintained in RPMI-1640 (Gibco, catalog N° 31800014) that was supplemented with 10% FBS and 0.5 μg/mL puromycin. The MCF-7 cell line (passage 7–9), obtained from ATCC, was grown in EMEM (ATCC, catalog N° 302003), supplemented with 10% FBS and 0.01 mg/mL insulin (Sigma-Aldrich, catalog I3536).

Immunophenotyping

Cells were harvested with TrypLE™ Select Enzyme (Gibco, catalog N° 12563011), and 10^5 cells were stained

with Alexa Fluor®-647 Rat IgG2a κ isotype control (BD Pharmigen, catalog N° 557857) or Alexa Fluor®-647 Rat anti-human CD49f (BD Pharmigen, catalog N° 562473). CD44 staining was performed with Brilliant Violet 421 Mouse anti-human CD44 (BD Horizon, catalog N° 5628790). Fluorescence was measured by flow cytometry (Attune NxT, Life Technologies), and the data were analyzed with FlowJo, version 8.7 (Tree Star Inc.).

Cell Viability

The effects of the drugs on viability were determined in cells that were in the exponential growth phase by MTS [3-(4,5-dimethylthiazol-2-yl)-5-(3-carboxymethoxyphenyl)-2-(4-sulfophenyl)-2H-tetrazolium, inner salt] assay. The amount of reduced tetrazolium salt was measured spectrophotometrically at 490 nm (Epoch, Biotek).

Cell Adhesion

Cell adhesion assays were performed as reported.[30,31] Briefly, 96-well microplates were coated with 20 µg/mL cold natural mouse laminin (Invitrogen, catalog N° 23017-015) and incubated overnight at 4°C. The wells were blocked with 10 mg/mL heat-denatured bovine serum albumin (BSA) for 1 h at 37°C.

Next, 3 x 10^5 cells from cultures after 12 h of serum starvation were preincubated with the selected drugs for 30 min at 37°C with shaking and then placed immediately into the laminin-coated wells and incubated for 20 min at 37°C. The wells were rinsed with PBS to remove nonadherent cells, and the number of viable attached cells was quantified by MTS reduction. As a control for the specificity of the system, CD49 blocking antibody (clone GoH3; BD Biosciences, catalog N° 562473) was included. The data were normalized to the signal that was obtained with the corresponding vehicle-treated cells.

Mammosphere Formation

Mammosphere formation assay was performed as reported.[15,28,32] Briefly, the cells were plated at low density (100 viable cells per well) on a 96-well ultra-low attachment plate (Corning Costar) with MammoCult medium and growth factors (StemCell Technologies, catalog N° 05620). The number of mammospheres with diameter >80 µm was quantified at day 7 by taking micrographs (Eclipse Ti-U microscopy, Nikon) and analyzing them in ImageJ.[33] In some experiments, the drugs were present during the 7-d incubation, whereas in other setups, the cells were pretreated for 24 h and the mammospheres were allowed to grow in drug-free medium. The results are expressed as the percentage of mammospheres with respect to the vehicle control.

Molecular Dynamics

MD simulations were performed with a heterodimeric model containing the seven-bladed beta-propeller domain of CD49f and the I-like and hybrid domains of β1 integrin, using Amber ff99SB force fields and the Amber 12 package.[34] The system was solvated using the TIP4P[35] water model in a periodic box, followed by the addition of Na^+ and Cl^- counterions to neutralize the systems. Ca^{2+} and Mg^{2+} ions were also included in the simulation as they are required for the proper function of this protein. The best pranlukast pose on CD49f was selected by clustering analysis of AutoDock4 data and used as a starting pose. Before the MD simulations, energy minimization and equilibration of the system were performed at constant temperature (300 K) and pressure (1 atm) using AmberTools. The MD simulations proceeded for 500 ns at the specified pressures and temperatures. Trajectory snapshots were taken every 10 ps for analysis. Root-mean-square deviation (RMSD) and Root-mean-square fluctuation (RMSF) of the backbone in the docked complex were analyzed in AmberTools 12. The hydrogen-bond formation between pranlukast and CD49f residues was determined by the implementation of the H-bond search module of Pytraj library (https://amber-md.github.io/pytraj). Interacting residues of the interface between α and β integrin subunits were determined by the Residue Interaction Network Generator (RING) server.[36] The binding-free energy (ΔG) was calculated on the last 40 ns of the MD simulation using the MM-GBSA method as implemented in AmberTools 12.[37] The calculation of entropy was not included in our protocol because it is time-consuming and exhibits a high degree of uncertainty.

Western Blot and Co-Immunoprecipitation

Cells were lysed in RIPA buffer (50 mM Tris-HCl, 0.1% SDS, 150 mM NaCl) supplemented with phosphatase inhibitors (2 mM EDTA, 15 mM NaF, 5 mM Na_3VO_4) and protease inhibitors (5 µg/mL leupeptin, 1 µg/mL pepstatin, 2 µg/mL aprotinin). Protein concentrations in the lysates were determined using the Pierce BCA Protein Assay Kit (Thermo Fisher Scientific, catalog N° 23225). Samples containing 30 µg of total protein were separated by SDS-PAGE and electroblotted onto PVDF membranes. After being blocked, the membranes were incubated with anti-

phospho-FAK (Tyr397; Millipore, catalog N° MAB1144), anti-phospho-AKT (Cell Signaling, catalog N° 92755), or anti-SOX2 (Abcam, catalog N° 97959), followed by an HRP-conjugated secondary antibody. To correct for differences in the amount of total protein loaded, the same membranes were stripped and reprobed with anti-FAK (Santa Cruz Biotechnology, catalog N° sc-1688), anti-AKT (Cell Signaling, catalog N° 92725), anti-β-actin (Santa Cruz Biotechnology, catalog N° sc-47778) or anti-α-tubulin (Santa Cruz Biotechnology, catalog N° sc-398103).

For co-immunoprecipitation assays, samples containing 1 mg of protein were incubated overnight at 4°C and constant agitation with anti-FAK and Protein A-agarose. After rinsing, the immune complexes were denatured with Laemmli buffer, subjected to SDS-PAGE, and electroblotted. Membranes were sequentially probed with anti-PI3K p110α (Santa Cruz Biotechnology, catalog N° SC-293172) and anti-FAK.

Protein bands were detected using SuperSignal West Femto Maximum Sensitivity Substrate Pierce ECL Western Blotting Substrate (Thermo Fisher Scientific, catalog N° 34095). Band intensities were measured in ImageJ[33] and data were normalized against the vehicle (DMSO).

SOX2 Promoter Transactivation

MDA-MB-231 cells that stably expressed Luc under the *SOX2* promoter were seeded into 24-well plates and incubated with drugs for 24 h. Then, the medium was removed, and the cells were lysed with 1% Triton X-100, 1 mM DTT in GME buffer for 10 min (room temperature). The homogenates were transferred to Eppendorf tubes, and 3 volumes of assay buffer (17 mM K_2PO_4, 1 mM DTT, and 2 mM ATP in GME buffer) were added. After the addition of luciferin (GOLDBIO, catalog N° LUCK-100), Luc activity was quantified as reported[29] (GloMax® 20/20; Promega). Data were normalized to the fraction of viable cells at each drug concentration.

Limiting-Dilution Xenotransplantation (LDT)

MDA-MB-231 cells expressing Luc2-eGFP[38] were treated with pranlukast (50 μM) or the corresponding vehicle for 24 h. Cells were detached, suspended in Dulbecco's PBS, mixed 1:1 with Matrigel® matrix (Corning, catalog N° 35621), and injected immediately into the thoracic mammary fat pad of 7–8-week-old female nu/nu mice (Cinvestav, Mexico). The tumor formation was examined by palpation at the injection site and by in vivo bioluminescence imaging as reported[38] on an IVIS XR system (Caliper Life Sciences). Bioluminescence data were analyzed using Living Image 3.0 (Caliper Life Sciences). At day 36 after injection, the mice were euthanized and necropsied to corroborate the presence of tumors.

Animal procedures were performed per Mexican guidelines for the production, care, and use of laboratory animals (NOM-062-ZOO-1999) and the National Institutes of Health Guide for the Care and Use of Laboratory Animals. The animal experiments were approved by the IACUC of the School of Medicine, UNAM (FMED/CI/JMO/102/2012).

Statistical Analyses

Half-maximal inhibitory concentration (IC_{50}) values were calculated by non-linear regression. Statistical significance was determined by one-way ANOVA or Kruskal–Wallis test. P values ≤0.05 are reported. GraphPad Prism (v6.0) was used to perform analyses. The estimation of CSC frequency was performed using ELDA software.[39]

Results

In silico Selection of CD49f Antagonists

We performed molecular docking using the β1-interacting domain of CD49f and 11,421 molecules from the InMan subset of the ZINC[12] database. The docking scores obtained with AutoDock Vina (Suppl. Figure 1A), Autodock (Suppl. Figure 1B), and their re-evaluation with DSX_089 (Suppl. Figure 1C–D), were normalized and used to generate a consensus Z-score (Suppl. Figure 1E). Of the compounds with lower consensus Z-scores, we selected five drugs with different reported targets (Suppl. Figure 1F): bromocriptine, montelukast, pranlukast, zosuquidar, and imatinib.

CD49f Antagonists Decrease Cell Adhesion to Laminin

For biological validation of our in silico findings, we analyzed the function of laminin receptors in breast cancer cells exposed to the drugs. We employed the triple-negative MDA-MB-231 cell line, which highly expresses CD49f (Suppl. Figure 2) and can efficiently adhere to laminin.[40] We found that >99% of MDA-MB-231 cells have high levels of membrane CD49f (Figure 1A), as reported.[41] We observed that all selected drugs dose-dependently decreased the MDA-MB-231 cell adhesion to laminin (Figure 1B–F). Montelukast, zosuquidar, and pranlukast had IC_{50} values between 10 and 30 μM, whereas those of imatinib and bromocriptine exceeded 50 μM. In these experiments, the

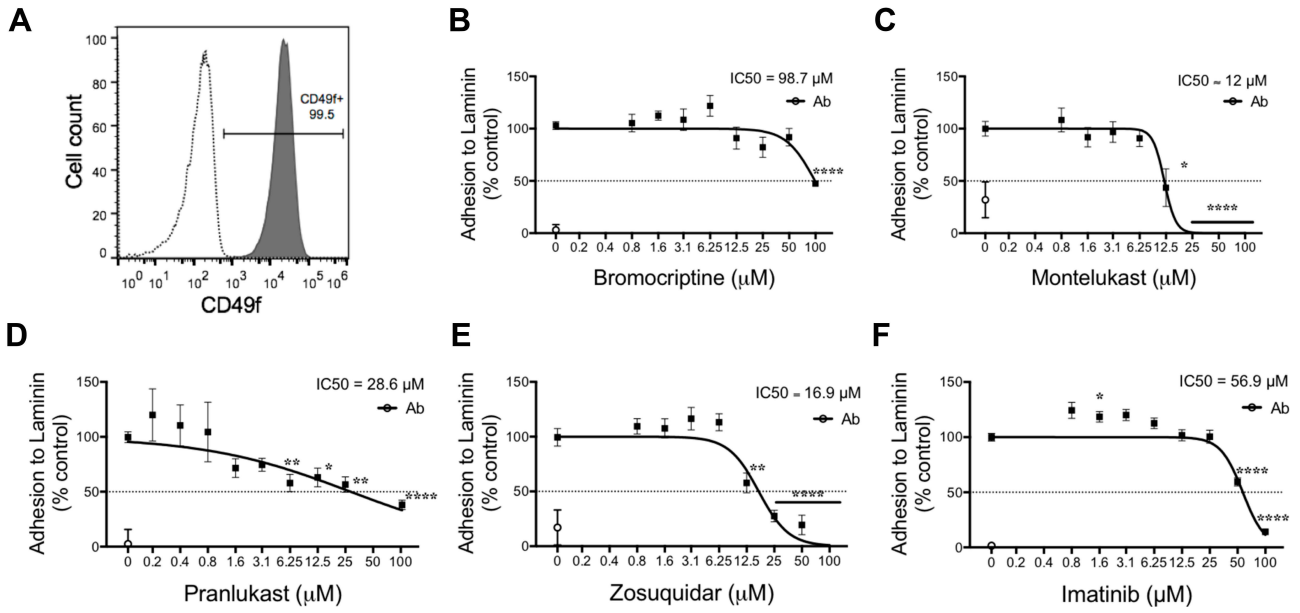

Figure 1 Effects of CD49f antagonists on CD49f adhesion to laminin. (**A**) Expression of CD49f in MDA-MB-231 cell line (gray histogram), assessed by FACS, versus its isotype control (white histogram). (**B–F**) Impact of selected compounds on MDA-MB-231 cell line adhesion to laminin. Graphs show the mean ± SEM of three independent experiments for bromocriptine (**B**), montelukast (**C**), pranlukast (**D**), zosuquidar (**E**), and imatinib (**F**). Half-maximal inhibitory concentration (IC_{50}) values were calculated by nonlinear regression and reported in Table 1. Statistical significance was determined by Dunnett´s test; P value <0.05 (*), <0.01 (**), <0.0001 (****).

treatment of cells with a CD49f-blocking monoclonal antibody (clone GoH3) abolished cell adhesion (open circles in Figure 1B– F), demonstrating that laminin adhesion of MDA-MB-231 cells depends on CD49f-containing integrins.

Pranlukast Impairs Mammosphere Formation Independently of Its Cytotoxic Effect

To determine the impact of CD49f antagonists on the fraction of stem/progenitor cells, we performed mammosphere assays. Continuous exposure of cells to bromocriptine, montelukast, pranlukast, zosuquidar, or imatinib significantly reduced the number of mammospheres formed by MDA-MB-231 cells (Figure 2A and Suppl. Figure 3). For comparison, we analyzed the cytotoxic effect of the drugs on tumor-bulk cells by performing cell viability assays in 2D cultures (Figure 2B). In these assays, only zosuquidar had an IC_{50} < 10 μM, and thus, only this drug should be classified as cytotoxic per NCI guidelines.[42]

The best candidate for further analysis was chosen by calculating a ratio between the IC_{50} values from both assays (Table 1). The concentration of pranlukast that was required to reduce the viability of 2D cultures was 10 times higher than what was needed to reduce clonogenicity, suggesting that this drug selectively affects breast CSCs.

Pranlukast Binding Induces Destabilization of α6β1 Heterodimer

To analyze the mechanism involved in pranlukast effects, we performed molecular dynamics (MD) simulations studying the drug´s interaction with a heterodimeric model composed of the seven-bladed beta-propeller domain of CD49f and the I-like and hybrid domains of β1 integrin. Root-mean-square deviation (RMSD) analysis showed that the heterodimeric complexes, with and without drug, reached equilibrium at ~150 ns (Figure 3A). Therefore, further analyses were performed with the 150 to 500 ns time frame. Pranlukast binding to CD49f was stable during the MD simulation. The drug–CD49f interaction was mediated by hydrophobic contacts, pi-pi stacking (Figure 3B), and hydrogen bonds (Figure 3C). We identified up to two simultaneous hydrogen bonds that involved Asn681, His702 or Ile703 in our model, which correspond to Asn300, His321 and Ile322 in the primary sequence of CD49f. The analysis of the root-mean-square fluctuation (RMSF) of backbone alpha carbons showed that pranlukast restricted the main backbone fluctuations of the propeller domain of CD49f (Figure 3D). Pranlukast induced conformational changes in the CD49f-binding site, reducing the fluctuations of the loop connecting C and D sheets of blade 5, but also in other regions of the protein that participate in the binding to the β subunit, such as in blades 2 and 3 (Figure 3E). Analysis of the α/β interface showed changes in the contacting

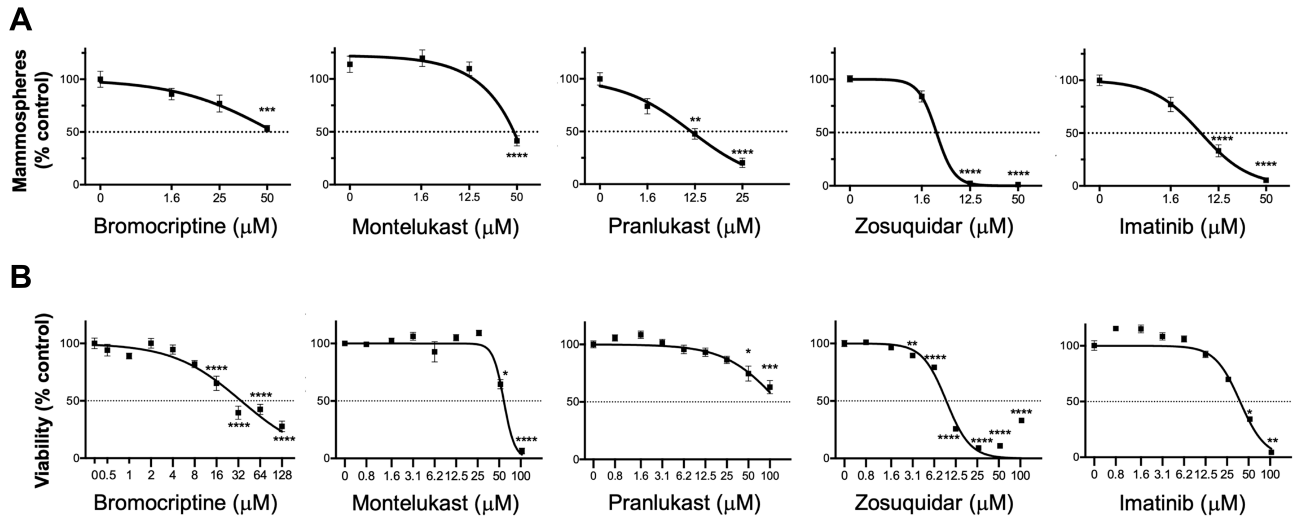

Figure 2 Selection of drugs with the highest CSC selectivity. Effect of CD49f antagonists on MDA-MB-231 mammosphere formation (**A**) and cell viability at 48 h, assessed by MTS assay (**B**). Graphs show mean ± SEM of three independent experiments. Half-maximal inhibitory concentration (IC50) values were calculated by nonlinear regression and reported in Table 1. Statistical significance was determined by Dunnett´s test; P value <0.05 (*), <0.01 (**), <0.001 (***), <0.0001 (****).

residues. For example, the surface on the I-like domain of β1 integrin had a different pattern of contacting residues in the presence of pranlukast (Figure 3F). Furthermore, the binding-free energy between the propeller domain of CD49f and the β1 subunit increases in presence of pranlukast (Figure 3G), indicating that the drug decreases the affinity between the subunits. This observation is consistent with the restricted conformational dynamics of the complex induced by pranlukast.

Pranlukast Effect on Other Laminin Receptors

To assess the specificity of pranlukast on CD49f, we performed laminin adhesion assays using MCF-7 breast cancer cells. Despite their low CD49f expression,[41] and Suppl. Figure 4A the cells efficiently adhered to laminin (Suppl. Figure 4B) as previously reported.[43,44] The addition of pranlukast (50 μM) did not affect the adhesion of MCF-7 cells to laminin (Suppl. Figure 4C), suggesting that the drug does not change the activity of other laminin receptors.

Table 1 Calculated IC_{50} Values from Viability or Mammosphere Assays and Ratio Between These Values

Compound	IC_{50} Mammosphere	IC_{50} Cell Viability	IC_{50} Cell Viability/ IC_{50} Mammosphere
Bromocriptine	61.1 μM	34.9 μM	0.57
Montelukast	48.4 μM	52.6 μM	1.09
Pranlukast	9.5 μM	>100 μM	**>10.53**
Zosuquidar	4.7 μM	9.1 μM	1.96
Imatinib	7.5 μM	36.5 μM	4.86

Note: Drug with higher ratio (bold) was selected for further studies.

Pranlukast Affects CD49f-Downstream Signaling

The effects of pranlukast on CD49f-mediated signaling were evaluated using adherent cultures of MDA-MB-231 cells exposed for 24 h. Subtoxic concentrations of pranlukast (≤50 μM; Suppl. Figure 5) decreased the integrin-dependent autophosphorylation of FAK at Tyr397. Pranlukast 12.5 μM reduced FAK phosphorylation without changes in total FAK, but 50 μM reduced both FAK phosphorylation as well as FAK expression (Figure 4A). Most importantly, blockage of CD49f with a specific monoclonal antibody only decreased FAK phosphorylation to 40% of control, indicating that in MDA-MB-231 cells, FAK activation is also mediated by other integrins, as reported.[45]

CD49f enhances radioresistance in breast cancer cells through the activation of the FAK-PI3K-AKT signaling pathway.[41] Thus, we studied the effect of pranlukast on the activation of FAK-downstream effectors. Pranlukast impaired the activity of PI3K, as demonstrated by the reduced phosphorylation of the PI3K-target AKT in cells treated with the drug (Figure 4B). The treatment also reduced the association of PI3K with FAK in co-immunoprecipitation assays (Figure 4C). Together, these results demonstrate that pranlukast affects the FAK/PI3K signal transduction pathway, supporting the idea that the drug impairs the function of CD49f-containing integrins.

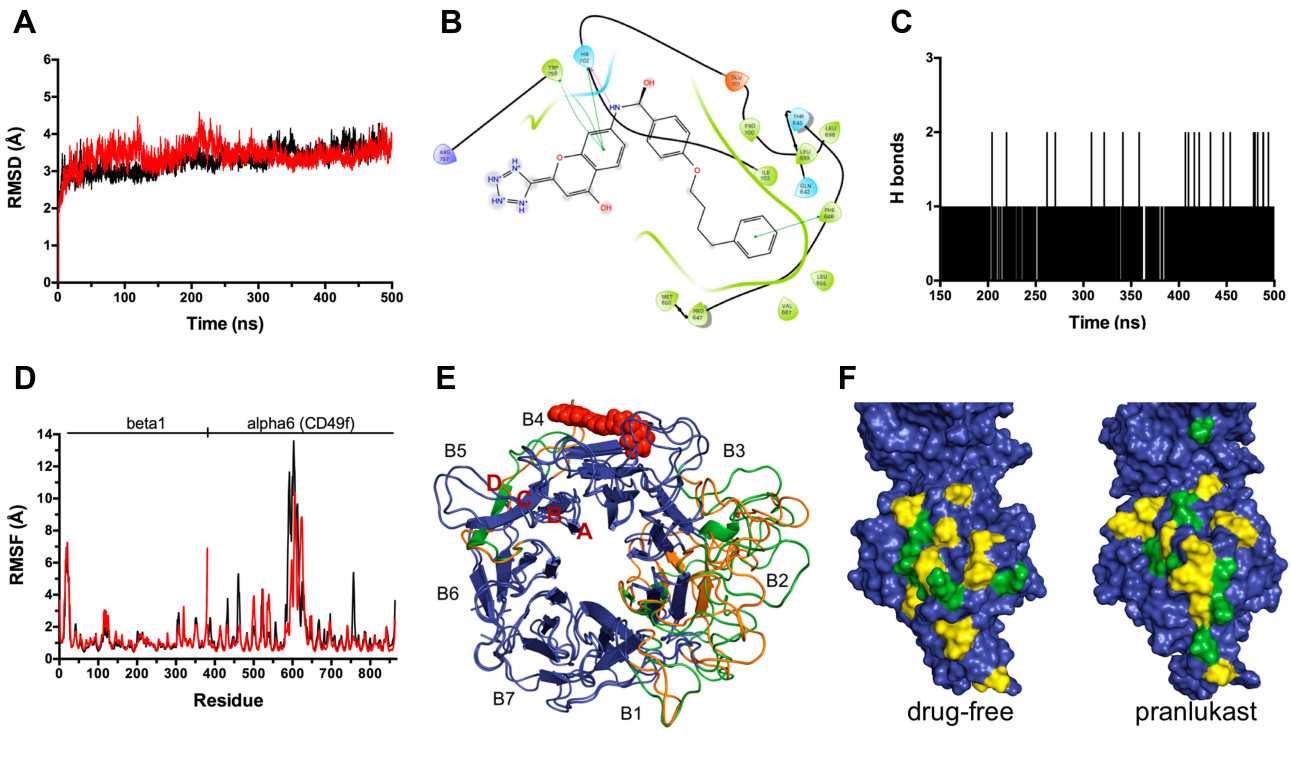

G

Complex	ΔG_{ele}	ΔG_{vdw}	ΔG_{nonpol}	ΔG_{pol}	$\Delta G_{bind,\ calc}$
$\alpha_6\beta_1$ drug-free	175.1798 (0.8)	-147.3897 (0.1)	-20.4644 (0.02)	-46.0847 (0.8)	**-38.7589** (0.15)
$\alpha_6\beta_1$-pranlukast	78.0856 (0.9)	-140.5671 (0.2)	-19.2863 (0.02)	49.0016 (0.9)	**-32.7662** (0.16)

Figure 3 Molecular dynamics analysis of pranlukast interaction with α6β1 integrin. (**A**) Root-mean-square deviation (RMSD) versus time plot for the backbone atoms in the absence (black line) or in the presence (red line) of pranlukast. (**B**) 2D representation of pranlukast-CD49f interactions. Residues in the binding site are represented as follows: acidic residues in orange, basic residues in violet, polar residues in blue, and hydrophobic residues in green. Green lines connecting residues to pranlukast indicate pi–pi stacking interactions and grey "clouds" on drug atoms indicate the solvent-exposed surface area. (**C**) Time evolution of the number of intermolecular hydrogen bonds formed between CD49f and pranlukast. (**D**) Root-mean-square fluctuation (RMSF) versus residue position for the backbone atoms of the target heterodimer in the absence (black line) or in the presence of pranlukast (red line). (**E**) Overlap of 3D models of the propeller domain of CD49f with or without pranlukast (in red spheres). Regions with no changes in backbone atoms between models are in blue, whereas regions with significant changes are in green for pranlukast-bound and orange for drug-free models, respectively. The number of the blades [B1–7] within the seven-bladed domain and the order of the beta-sheets [A–D] within blades is annotated. (**F**) Surface representation of the interface of β1 integrin with or without pranlukast. Residues making hydrophobic contacts or hydrogen bonds with CD49f are shown in yellow and green, respectively. (**G**) Binding-free energy calculated from MD simulation ($\Delta G_{bind,\ calc}$). $\Delta G_{bind,\ calc}$ for the drug free- and pranlukast bound-complexes (bold values) were calculated considering the energy contributed by electrostatic (ΔG_{ele}), van der Waals (ΔG_{vdw}), hydrophobic (ΔG_{nonpol}), and polar (ΔG_{pol}) forces. The values in parenthesis correspond to the standard error of mean.

Pranlukast Affects Stemness and Reduces the CSC Frequency

The effects of pranlukast on stemness were evaluated after exposing adherent cultures of MDA-MB-231 cells for 24 h to the drug (Figure 5A). Preincubation of MDA-MB-231 cells with 50 µM of pranlukast significantly reduced the mammosphere-forming efficiency under drug-free conditions (Figure 5B). Further, pranlukast significantly reduced the expression of the CSC marker CD44 (Figure 5C) and the pluripotency protein SOX2 (Figure 5D), as well as *SOX2* promoter transactivation (Figure 5E).

The effect of pranlukast on tumor onset was assessed by limiting dilution xenotransplantation. We injected groups of nu/nu mice with different numbers of vehicle- or pranlukast-treated cells. The bioluminescence at time 0 showed that paired groups were homogeneously injected with live cells (P>0.05; Student´s *t*-test). The fraction of tumor-free mice in each group was quantified 5 weeks later (Figure 5F). For example, the injection of 2000 pranlukast-treated cells generated tumors in 3 out of 8 mice, compared with 6 out of 8 tumors produced by vehicle-treated cells (Figure 5G). The limiting dilution

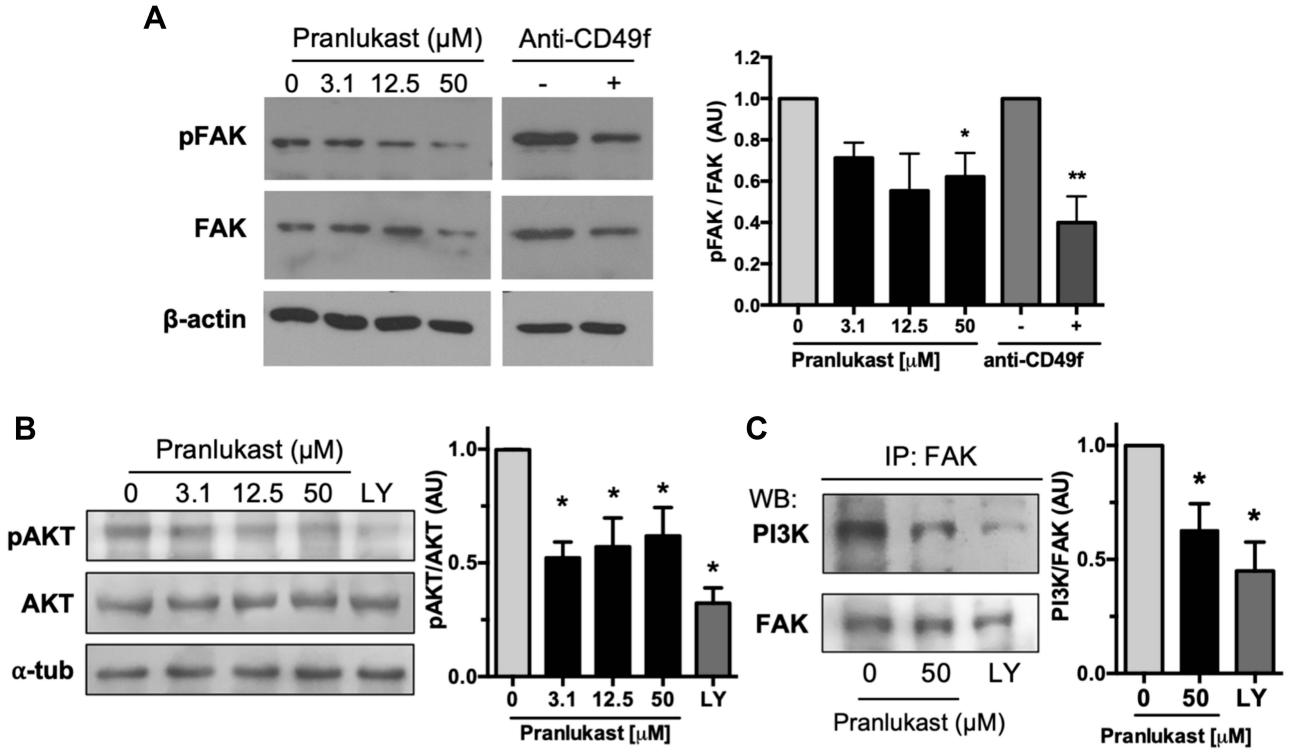

Figure 4 Effect of pranlukast on FAK signaling. (**A**) Representative Western blot evaluating the Tyr397 phosphorylation of FAK (pFAK) and the corresponding analysis of the pFAK/FAK ratio from three independent experiments. (**B**) Representative Western blot analyzing the phosphorylation of the PI3K substrate AKT and the densitometric analysis from four independent experiments. The PI3K inhibitor LY294002 [LY; 5 μM] was employed as a control. (**C**) Western blot against PI3K or FAK in samples immunoprecipitated with anti-FAK. Graph shows densitometric analysis from four independent experiments. All statistical analyses were performed using Dunnett's test; P value <0.05 (*), <0.01 (**).
Abbreviation: AU, arbitrary units.

analysis of pooled results showed a significant 3.7-fold reduction in the frequency of tumor-initiating cells after pranlukast treatment (Figure 5H). Thus, pranlukast reduced stemness signaling and impaired cellular functions that define CSC, demonstrating that it declines the CSC population.

Discussion

Integrin dimerization is crucial for the generation of its ligand-binding domain and, consequently, for integrin activation and clustering.[20,21] Disruption of dimerization by peptides or monoclonal antibodies blocks integrin clustering and integrin-mediated adhesion.[46–48] Targeting protein–protein interactions (PPIs) with small compounds has emerged as a novel and viable approach in modern drug discovery.[49] Thus, we hypothesized that altering PPIs in CD49f-containing integrins by using pharmochemicals would impair their activity.

By molecular docking, we identified 20 compounds with high binding potential to a druggable pocket within the seven-bladed beta-propeller domain of CD49f. Of these potential antagonists, we focused on five drugs with known pharmacokinetics and pharmacodynamics. Analyzing new biological activities of drugs with reported therapeutic use (drug repurposing) is a strategy that reduces the time between the discovery of a new application and clinical translation.[50,51] Our team used a similar strategy to identify etoposide as an antagonist of CD44.[28]

The five selected drugs – bromocriptine, montelukast, pranlukast, zosuquidar, and imatinib – inhibited the adhesion of $CD49f^{+}$ breast cancer cells to laminin with various potencies. Our data showed that the adhesion of MDA-MB -231 cells highly depends on CD49f, as demonstrated by the use of a monoclonal anti-CD49f. These results indicate that the selected pocket has functional relevance and could be used to design new antagonists for CD49f or other homologous integrins.

CD49f is central in maintaining the stemness[7,11,12,14,17] but is dispensable for the survival of non-CSCs in vitro.[9,10] Consequently, CD49f blockade is expected to affect clonogenicity with a minor impact on global cell viability. Hence, our subsequent screening compared the effect of

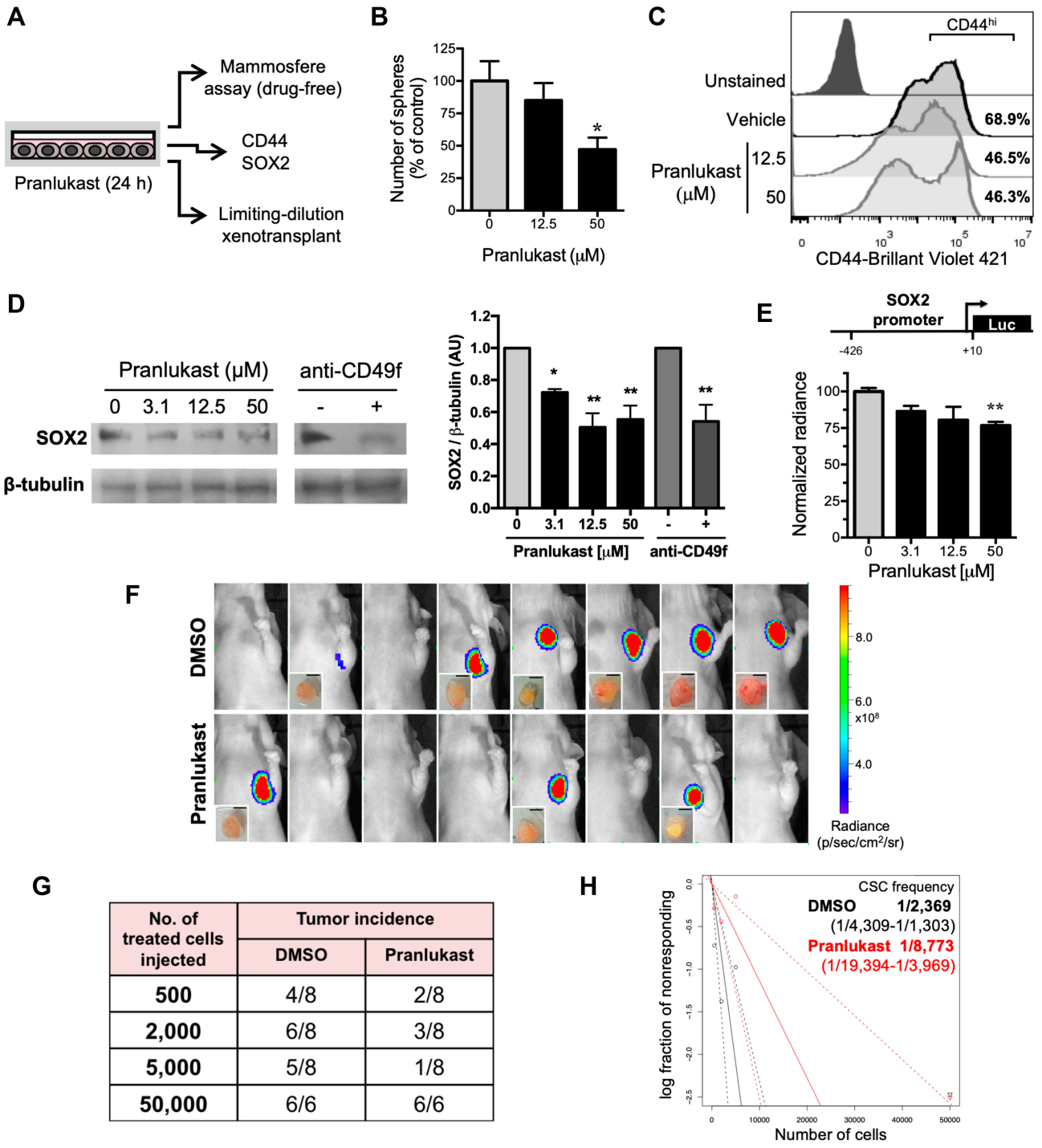

No. of treated cells injected	Tumor incidence	
	DMSO	Pranlukast
500	4/8	2/8
2,000	6/8	3/8
5,000	5/8	1/8
50,000	6/6	6/6

Figure 5 Effect of pranlukast on breast cancer cell stemness. (**A**) Experimental strategy. (**B**) Viable MDA-MB-231 cells previously exposed to pranlukast for 24 h were seeded to test their capacity to form mammospheres in the absence of the drug. Graphs show the mean number of mammospheres ± SD from three independent experiments. (**C**) Analysis of CD44 expression by flow cytometry. The annotated percentages correspond to $CD44^{hi}$ population. A representative experiment from 2 is shown. (**D**) Representative Western blot analyzing SOX2 expression. Graph represents the mean ± SEM from three independent experiments. (**E**) Analysis of *SOX2* promoter transactivation by luciferase assay. Values are mean ± SEM from four independent experiments. Scheme above graph shows the promoter size in the construct. Statistical significance in (**B**), (**D**), and (**E**) was determined by Dunnett´s test; P value <0.05 (*), <0.01 (**). AU: arbitrary units. (**F**) Tumor formation in nude mice injected with 2000 cells in the vehicle (upper row) or pranlukast (lower row) groups. The presence of tumors was evaluated 36 days postinjection by bioluminescence quantification and dissection. Insets show the dissected tumors; scale bar = 3 mm. (**G**) Tumor incidence in groups of mice xenotransplanted with vehicle- or pranlukast-treated cells. (**H**) Log-fraction plot of the limiting dilution model fitted to the data shown in (**E**). The CSC frequency and the corresponding 95% confidence intervals (dotted lines and fractions in parenthesis) were calculated using ELDA software. The CSC frequency was significantly different among treatments (P=0.0044; chi-square test).

each drug on mammosphere formation, a functional estimation of the number of CSCs,[15,52] *versus* its effect on the viability of adherent cultures, which are enriched in non-stem cells.[53,54] Pranlukast decreased the number of mammospheres with limited cytotoxicity to adherent cultures, supporting that it selectively targets the CSC pool.

Pranlukast binding mode to CD49f was further characterized by MD simulations. Those experiments were performed with a heterodimeric model that included key domains for the ligand-binding activity of integrins.[21,46,55] Pranlukast stably bound to CD49f in a region that includes residues that participate in or lie near the reported β-subunit interaction site in homologous proteins. In the αV integrin, the template used for our CD49f model, the contacting residues with the β3 subunit reside primarily in blades 3–5 of the seven-bladed beta-propeller domain.[55] Accordingly, pranlukast binding to CD49f reduced the affinity for the β subunit. Furthermore, our results suggest that pranlukast constrains the conformational dynamics of the protein, which is crucial to regulate the activation state of the heterodimer.[46]

We also analyzed the effect of pranlukast in CD49f-downstream signaling using MDA-MB-231 cells. FAK, a non-receptor tyrosine kinase, mediates signal transduction by CD49f[12] and has been associated with aggressiveness in triple-negative breast tumors.[56] FAK ablation in mammary epithelial cells delays tumorigenesis and reduces the pool of CSC in mammary tumors.[57] Fittingly, FAK inhibition blocks metastatic ability and stemness in triple-negative breast cancer cells.[58] We found that pranlukast decreased the integrin-dependent autophosphorylation of FAK at Tyr397, which is a surrogate measurement of FAK activation.[59] CD49f-FAK activity stimulates the PI3K/AKT pathway leading to its hyperactivation in triple-negative tumors[60] and in breast CSCs.[61] We showed that pranlukast reduced FAK-PI3K interaction and AKT phosphorylation, corroborating that CD49f-activated signaling was impaired by the drug.

Previous studies have demonstrated that PI3K/AKT blockage induces CSC-differentiation in breast cancer cells.[62] Thus, we studied whether pranlukast effects on CSC were reversible using an experimental design reported by Gupta and colleagues.[63] Short-term exposure to pranlukast reduced the fraction of mammosphere-initiating cells in drug-free cultures as well as the number of tumor-initiating cells in vivo. These changes in the CSC pool were corroborated by quantifying the expression of two proteins that participate in the maintenance of stemness, expression of EMT markers, invasiveness, and metastatic capability: SOX2[64–66] and CD44.[67] SOX2 is a target of CD49f-activated signaling[11] and its downregulation is sufficient to diminish the pool of breast CSCs.[66,68,69] Pranlukast reduced SOX2 protein level with a modest decrease in *SOX2* promoter transactivation, suggesting that the drug affects the post-translational modifications and the stability of the protein. SOX2 expression positively correlates with that of CD44 in clinical samples;[70] accordingly, we found a reduction of the $CD44^{hi}$ population in pranlukast-treated cells. Since SOX2 and CD44 expression induce chemoresistance in MDA-MB-231 cells,[71] future studies would analyze the effect of pranlukast in the response to cytotoxic drugs.

Pranlukast, like montelukast and zafirlukast, belongs to the group of CysLTR antagonists, which are used to treat chronic bronchial asthma.[72] Although pranlukast and montelukast were selected as potential CD49f antagonists by our in silico screen, our results show that they have dissimilar pharmacological behaviors, as described.[72] For example, both drugs inhibit CysLTR1-mediated lung colonization by cancer cells, but only pranlukast impairs capillary permeability and cancer cell extravasation in the brain.[73] Further, pranlukast was recently reported to act as an agonist of Raf1 kinase inhibitory protein,[74] which is usually absent in metastatic cancer cells and is considered a metastasis suppressor.[75] These data suggest that pranlukast can target multiple proteins, and we hereby report that CD49f should be considered one of such targets.

Conclusions

Our results identified pranlukast, a drug that is administered to asthmatic patients, as a CD49f-blocking agent with functional effects on the breast CSC pool, likely caused by altered FAK- and SOX2-signaling. Because the pharmacokinetics and toxicology of this drug are known, we recommend evaluating pranlukast as an adjuvant therapy for breast cancer patients to reduce drug resistance and tumor recurrence.

Abbreviations

CSC, cancer stem cell; CysLTR, cysteinyl leukotriene receptor 1; DMSO, dimethyl sulfoxide; FAK, focal adhesion kinase; FDA, Food and Drug Administration, USA; IC_{50}, half-maximal inhibitory concentration; MD, molecular dynamics; NCI, National Cancer Institute, USA; PI3K, phosphatidylinositol 3-kinase; RMSD, root-mean-square deviation; RMSF, root-mean-square fluctuation; AU, arbitrary units.

Ethics Approval

Animal procedures were performed per Mexican guidelines for the production, care, and use of laboratory

animals (NOM-062-ZOO-1999) and the National Institutes of Health Guide for the Care and Use of Laboratory Animals (NIH Publications No. 80-23, revised 1978). The animal experiments were approved by the IACUC of "Facultad de Medicina, UNAM" (FMED/CI/JMO/102/2012).

Acknowledgments

This work was partially carried out with the equipment of the National Laboratory for Specialized Services of Investigation, Development and Innovation (I+D+i) for Pharma Chemicals and Biotechnological products, LANSEIDI-FarBiotec-CONACyT, which is part of the Research and Development in Bioprocess Unit (UDIBI)-IPN. We thank Andrea Rodríguez-Moreno, Sandra Guerrero-Rodríguez, Mireya Velázquez-Paniagua, Homero Gómez-Velasco, Luis A. Valencia-Flores, and Israel Castro-Cruz for technical assistance and Ms. Josefina Bolado, Head of the Scientific Paper Translation Department from the Research Division, School of Medicine, UNAM, for language editing. We also thank the support of "Programa de Becas Posdoctorales, DGAPA-UNAM". Charmina Aguirre-Alvarado is currently affiliated with the Unit for Research in Immunology and Infectology, CMN "La Raza", Instituto Mexicano del Seguro Social, Mexico City, Mexico.

Author Contributions

All authors made substantial contributions to conception and design, acquisition of data, or analysis and interpretation of data; took part in drafting the article or revising it critically for important intellectual content; gave final approval of the version to be published; and agree to be accountable for all aspects of the work.

Funding

This work was supported by CONACyT 221103 and INFR-2014-01-225313, PAPIIT UNAM IN228616 and IN219719 (M.A.V-V.), UDIMEB (S.M.P-T.), and POSDOC DGAPA-UNAM (D.C-A.). A.J.R-M. and F.C-M. are recipients of graduate scholarships from CONACyT.

Disclosure

This paper was presented at the 2018 NCRI Conference as a poster presentation with interim findings. The poster's abstract was published in "Selected Abstracts from the 2018 NCRI Cancer Conference of National Cancer Research Institute" in *British Journal of Cancer*; 2018;119:46; https://doi.org/10.1038/s41416-018-0299-z. Dr Inés Velázquez-Quesada reports a patent for pranlukast as an antagonist of CD49f and derived uses pending. Dr Aliesha González-Arenas reports a patent pending: Mx/a/2018/014001. Dr Marco A Velasco-Velázquez reports grants from CONACYT, and PAPIIT UNAM and Dr. Diana Casique-Aguirre reports personal fees from POSDOC DGAPA-UNAM during the conduct of the study; in addition, they have a patent pending: MX/a/2018/014001. Sonia M Pérez-Tapia was employed by the National Laboratory for Specialized Services of Investigation, Development and Innovation (I+D+i) for Pharma Chemicals and Biotechnological Products, LANSEIDI-FarBiotec-CONACyT, during the study. The authors report no other conflicts of interest in this work.

References

1. Stewart B, Wild CP *World Cancer Report 2014*. Lyon, France: International Agency for Research on Cancer; 2014.
2. Population Reference Bureau. *2012 World Population Data Sheet*. Population Reference Bureau. ed.. Washington, DC: Population Reference Bureau; 2012.
3. Ahmad A. Pathways to breast cancer recurrence. *ISRN Oncol*. 2013;2013:290568. doi:10.1155/2013/290568
4. Velasco-Velázquez MA, Homsi N, De La Fuente M, Pestell RG. Breast cancer stem cells. *Int J Biochem Cell Biol*. 2012;44(4):573–577. doi:10.1016/j.biocel.2011.12.020
5. Jiang FX, Georges-Labouesse E, Harrison LC. Regulation of laminin 1-induced pancreatic beta-cell differentiation by alpha6 integrin and alpha-dystroglycan. *Mol Med*. 2001;7(2):107–114. doi:10.1007/BF03401944
6. Nishiuchi R, Takagi J, Hayashi M, et al. Ligand-binding specificities of laminin-binding integrins: a comprehensive survey of laminin-integrin interactions using recombinant alpha3beta1, alpha6-beta1, alpha7beta1 and alpha6beta4 integrins. *Matrix Biol*. 2006;25(3):189–197. doi:10.1016/j.matbio.2005.12.001
7. Brooks DLP, Schwab LP, Krutilina R, et al. ITGA6 is directly regulated by hypoxia-inducible factors and enriches for cancer stem cell activity and invasion in metastatic breast cancer models. *Mol Cancer*. 2016;15:26. doi:10.1186/s12943-016-0510-x
8. Shaw LM, Chao C, Wewer UM, Mercurio AM. Function of the integrin alpha 6 beta 1 in metastatic breast carcinoma cells assessed by expression of a dominant-negative receptor. *Cancer Res*. 1996;56(5):959–963.
9. Wewer UM, Shaw LM, Albrechtsen R, Mercurio AM. The integrin alpha 6 beta 1 promotes the survival of metastatic human breast carcinoma cells in mice. *Am J Pathol*. 1997;151(5):1191–1198.
10. Vassilopoulos A, Chisholm C, Lahusen T, Zheng H, Deng CX. A critical role of CD29 and CD49f in mediating metastasis for cancer-initiating cells isolated from a Brca1-associated mouse model of breast cancer. *Oncogene*. 2014;33(47):5477–5482. doi:10.1038/onc.2013.516
11. Yu K-R, Yang S-R, Jung J-W, et al. CD49f enhances multipotency and maintains stemness through the direct regulation of OCT4 and SOX2. *Stem Cells*. 2012;30(5):876–887. doi:10.1002/stem.1052
12. Goel HL, Pursell B, Chang C, et al. GLI1 regulates a novel neuropilin-2/α6β1 integrin based autocrine pathway that contributes to breast cancer initiation. *EMBO Mol Med*. 2013;5(4):488–508. doi:10.1002/emmm.201202078
13. To K, Fotovati A, Reipas KM, et al. Y-box binding protein-1 induces the expression of CD44 and CD49f leading to enhanced self-renewal, mammosphere growth, and drug resistance. *Cancer Res*. 2010;70(7):2840–2851. doi:10.1158/0008-5472.CAN-09-3155

14. Goel HL, Gritsko T, Pursell B, et al. Regulated splicing of the α6 integrin cytoplasmic domain determines the fate of breast cancer stem cells. *Cell Rep*. 2014;7(3):747–761. doi:10.1016/j.celrep.2014.03.059
15. Dontu G, Abdallah WM, Foley JM, et al. In vitro propagation and transcriptional profiling of human mammary stem/progenitor cells. *Genes Dev*. 2003;17(10):1253–1270. doi:10.1101/gad.1061803
16. Pece S, Tosoni D, Confalonieri S, et al. Biological and molecular heterogeneity of breast cancers correlates with their cancer stem cell content. *Cell*. 2010;140(1):62–73. doi:10.1016/j.cell.2009.12.007
17. Cariati M, Naderi A, Brown JP, et al. Alpha-6 integrin is necessary for the tumourigenicity of a stem cell-like subpopulation within the MCF7 breast cancer cell line. *Int J Cancer*. 2008;122(2):298–304. doi:10.1002/ijc.23103
18. Perdih A, Sollner Dolenc M. Small molecule antagonists of integrin receptors. *CMC*. 2010;17(22):2371–2392. doi:10.2174/092986710791698558
19. Goodman SL, Picard M. Integrins as therapeutic targets. *Trends Pharmacol Sci*. 2012;33(7):405–412. doi:10.1016/j.tips.2012.04.002
20. Millard M, Odde S, Neamati N. Integrin targeted therapeutics. *Theranostics*. 2011;1:154–188. doi:10.7150/thno/v01p0154
21. Ley K, Rivera-Nieves J, Sandborn WJ, Shattil S. Integrin-based therapeutics: biological basis, clinical use and new drugs. *Nat Rev Drug Discov*. 2016;15(3):173–183. doi:10.1038/nrd.2015.10
22. Irwin JJ, Sterling T, Mysinger MM, Bolstad ES, Coleman RG. ZINC: a free tool to discover chemistry for biology. *J Chem Inf Model*. 2012;52(7):1757–1768. doi:10.1021/ci3001277
23. Sali A, Blundell TL. Comparative protein modelling by satisfaction of spatial restraints. *J Mol Biol*. 1993;234(3):779–815. doi:10.1006/jmbi.1993.1626
24. Volkamer A, Kuhn D, Grombacher T, Rippmann F, Rarey M. Combining global and local measures for structure-based druggability predictions. *J Chem Inf Model*. 2012;52(2):360–372. doi:10.1021/ci200454v
25. Trott O, Olson AJ. AutoDock Vina: improving the speed and accuracy of docking with a new scoring function, efficient optimization, and multithreading. *J Comput Chem*. 2010;31(2):455–461. doi:10.1002/jcc.21334
26. Morris GM, Huey R, Lindstrom W, et al. AutoDock4 and AutoDockTools4: automated docking with selective receptor flexibility. *J Comput Chem*. 2009;30(16):2785–2791. doi:10.1002/jcc.21256
27. Neudert G, Klebe G. DSX: a knowledge-based scoring function for the assessment of protein-ligand complexes. *J Chem Inf Model*. 2011;51(10):2731–2745. doi:10.1021/ci200274q
28. Aguirre-Alvarado C, Segura-Cabrera A, Velázquez-Quesada I, et al. Virtual screening-driven repositioning of etoposide as CD44 antagonist in breast cancer cells. *Oncotarget*. 2016;7(17):23772–23784. doi:10.18632/oncotarget.8180
29. Wu K, Jiao X, Li Z, et al. Cell fate determination factor Dachshund reprograms breast cancer stem cell function. *J Biol Chem*. 2011;286(3):2132–2142. doi:10.1074/jbc.M110.148395
30. Humphries MJ. Cell adhesion assays. *MB*. 2001;18(1):57–62. doi:10.1385/MB:18:1:57
31. Velasco-Velázquez MA, Agramonte-Hevia J, Barrera D, et al. 4-Hydroxycoumarin disorganizes the actin cytoskeleton in B16-F10 melanoma cells but not in B82 fibroblasts, decreasing their adhesion to extracellular matrix proteins and motility. *Cancer Lett*. 2003;198(2):179–186. doi:10.1016/s0304-3835(03)00333-1
32. Lombardo Y, de Giorgio A, Coombes CR, Stebbing J, Castellano L. Mammosphere formation assay from human breast cancer tissues and cell lines. *J Vis Exp*. 2015;(97). doi:10.3791/52671
33. Schneider CA, Rasband WS, Eliceiri KW. NIH image to imageJ: 25 years of image analysis. *Nat Methods*. 2012;9(7):671–675. doi:10.1038/nmeth.2089
34. Case DA, Cheatham TE, Darden T, et al. The Amber biomolecular simulation programs. *J Comput Chem*. 2005;26(16):1668–1688. doi:10.1002/jcc.20290
35. Zlenko DV. Расчет коэффициента самодиффузии tip4p-воды [Diffusion factor calculation for TIP4P model of water]. *Biofizika*. 2012;57(2):197–204. Article in Russian.
36. Piovesan D, Minervini G, Tosatto SCE. The RING 2.0 web server for high quality residue interaction networks. *Nucleic Acids Res*. 2016;44(W1):W367–74. doi:10.1093/nar/gkw315
37. Salomon-Ferrer R, Case DA, Walker RC. An overview of the Amber biomolecular simulation package. *WIREs Comput Mol Sci*. 2013;3(2):198–210. doi:10.1002/wcms.1121
38. Velasco-Velázquez M, Jiao X, De La Fuente M, et al. CCR5 antagonist blocks metastasis of basal breast cancer cells. *Cancer Res*. 2012;72(15):3839–3850. doi:10.1158/0008-5472.CAN-11-3917
39. Hu Y, Smyth GK. ELDA: extreme limiting dilution analysis for comparing depleted and enriched populations in stem cell and other assays. *J Immunol Methods*. 2009;347(1–2):70–78. doi:10.1016/j.jim.2009.06.008
40. Popolin CP, Reis JPB, Becceneri AB, et al. Cytotoxicity and anti-tumor effects of new ruthenium complexes on triple negative breast cancer cells. *PLoS One*. 2017;12(9):e0183275. doi:10.1371/journal.pone.0183275
41. Hu T, Zhou R, Zhao Y, Wu G. Integrin α6/Akt/Erk signaling is essential for human breast cancer resistance to radiotherapy. *Sci Rep*. 2016;6:33376. doi:10.1038/srep33376
42. Boyd MR, Paull KD. Some practical considerations and applications of the national cancer institute in vitro anticancer drug discovery screen. *Drug Dev Res*. 1995;34(2):91–109. doi:10.1002/ddr.430340203
43. Plopper GE, Domanico SZ, Cirulli V, Kiosses WB, Quaranta V. Migration of breast epithelial cells on Laminin-5: differential role of integrins in normal and transformed cell types. *Breast Cancer Res Treat*. 1998;51(1):57–69. doi:10.1023/a:1006086218174
44. Pal S, Moulik S, Dutta A, Chatterjee A. Extracellular matrix protein laminin induces matrix metalloproteinase-9 in human breast cancer cell line mcf-7. *Cancer Microenviron*. 2014;7(1–2):71–78. doi:10.1007/s12307-014-0146-6
45. Taherian A, Li X, Liu Y, Haas TA. Differences in integrin expression and signaling within human breast cancer cells. *BMC Cancer*. 2011;11:293. doi:10.1186/1471-2407-11-293
46. Gahmberg CG, Fagerholm SC, Nurmi SM, Chavakis T, Marchesan S, Grönholm M. Regulation of integrin activity and signalling. *Biochim Biophys Acta*. 2009;1790(6):431–444. doi:10.1016/j.bbagen.2009.03.007
47. Laplantine E, Maurer P, Vallar L, et al. The integrin β1 subunit cytoplasmic tail forms oligomers: a potential role in β1 integrin clustering. *Biol Cell*. 2002;94(6):375–387. doi:10.1016/S0248-4900(02)00009-6
48. Brinkerhoff CJ, Linderman JJ. Integrin dimerization and ligand organization: key components in integrin clustering for cell adhesion. *Tissue Eng*. 2005;11(5–6):865–876. doi:10.1089/ten.2005.11.865
49. Arkin MR, Tang Y, Wells JA. Small-molecule inhibitors of protein-protein interactions: progressing toward the reality. *Chem Biol*. 2014;21(9):1102–1114. doi:10.1016/j.chembiol.2014.09.001
50. Li J, Zheng S, Chen B, Butte AJ, Swamidass SJ, Lu Z. A survey of current trends in computational drug repositioning. *Brief Bioinformatics*. 2016;17(1):2–12. doi:10.1093/bib/bbv020
51. Würth R, Thellung S, Bajetto A, Mazzanti M, Florio T, Barbieri F. Drug-repositioning opportunities for cancer therapy: novel molecular targets for known compounds. *Drug Discov Today*. 2016;21(1):190–199. doi:10.1016/j.drudis.2015.09.017
52. Smart CE, Morrison BJ, Saunus JM, et al. In vitro analysis of breast cancer cell line tumourspheres and primary human breast epithelia mammospheres demonstrates inter- and intrasphere heterogeneity. *PLoS One*. 2013;8(6):e64388. doi:10.1371/journal.pone.0064388
53. Yousefnia S, Ghaedi K, Seyed Forootan F, Nasr Esfahani MH. Characterization of the stemness potency of mammospheres isolated from the breast cancer cell lines. *Tumour Biol*. 2019;41(8):1010428319869101. doi:10.1177/1010428319869101

54. Zhang X, Li F, Zheng Y, et al. Propofol reduced mammosphere formation of breast cancer stem cells via PD-L1/nanog in vitro. *Oxid Med Cell Longev*. 2019;2019:9078209. doi:10.1155/2019/9078209
55. Xiong JP, Stehle T, Diefenbach B, et al. Crystal structure of the extracellular segment of integrin alpha Vbeta3. *Science*. 2001;294(5541):339–345. doi:10.1126/science.1064535
56. Golubovskaya VM, Ylagan L, Miller A, et al. High focal adhesion kinase expression in breast carcinoma is associated with lymphovascular invasion and triple-negative phenotype. *BMC Cancer*. 2014;14:769. doi:10.1186/1471-2407-14-769
57. Luo M, Fan H, Nagy T, et al. Mammary epithelial-specific ablation of the focal adhesion kinase suppresses mammary tumorigenesis by affecting mammary cancer stem/progenitor cells. *Cancer Res*. 2009;69(2):466–474. doi:10.1158/0008-5472.CAN-08-3078
58. Kolev VN, Tam WF, Wright QG, et al. Inhibition of FAK kinase activity preferentially targets cancer stem cells. *Oncotarget*. 2017;8(31):51733–51747. doi:10.18632/oncotarget.18517
59. Schaller MD, Hildebrand JD, Shannon JD, Fox JW, Vines RR, Parsons JT. Autophosphorylation of the focal adhesion kinase, pp125FAK, directs SH2-dependent binding of pp60src. *Mol Cell Biol*. 1994;14(3):1680–1688. doi:10.1128/mcb.14.3.1680
60. López-Knowles E, O'Toole SA, McNeil CM, et al. PI3K pathway activation in breast cancer is associated with the basal-like phenotype and cancer-specific mortality. *Int J Cancer*. 2010;126(5):1121–1131. doi:10.1002/ijc.24831
61. Hardt O, Wild S, Oerlecke I, et al. Highly sensitive profiling of CD44+/CD24- breast cancer stem cells by combining global mRNA amplification and next generation sequencing: evidence for a hyperactive PI3K pathway. *Cancer Lett*. 2012;325(2):165–174. doi:10.1016/j.canlet.2012.06.010
62. Kim H, Lin Q, Glazer PM, Yun Z. The hypoxic tumor microenvironment in vivo selects the cancer stem cell fate of breast cancer cells. *Breast Cancer Res*. 2018;20(1):16. doi:10.1186/s13058-018-0944-8
63. Gupta PB, Onder TT, Jiang G, et al. Identification of selective inhibitors of cancer stem cells by high-throughput screening. *Cell*. 2009;138(4):645–659. doi:10.1016/j.cell.2009.06.034
64. Weina K, Utikal J. SOX2 and cancer: current research and its implications in the clinic. *Clin Transl Med*. 2014;3:19. doi:10.1186/2001-1326-3-19
65. Liu K, Xie F, Gao A, et al. SOX2 regulates multiple malignant processes of breast cancer development through the SOX2/miR-181a-5p, miR-30e-5p/TUSC3 axis. *Mol Cancer*. 2017;16(1):62. doi:10.1186/s12943-017-0632-9
66. Mukherjee P, Gupta A, Chattopadhyay D, Chatterji U. Modulation of SOX2 expression delineates an end-point for paclitaxel-effectiveness in breast cancer stem cells. *Sci Rep*. 2017;7(1):9170. doi:10.1038/s41598-017-08971-2
67. Chanmee T, Ontong P, Kimata K, Itano N. Key roles of hyaluronan and its CD44 receptor in the stemness and survival of cancer stem cells. *Front Oncol*. 2015;5:180. doi:10.3389/fonc.2015.00180
68. Stolzenburg S, Rots MG, Beltran AS, et al. Targeted silencing of the oncogenic transcription factor SOX2 in breast cancer. *Nucleic Acids Res*. 2012;40(14):6725–6740. doi:10.1093/nar/gks360
69. Piva M, Domenici G, Iriondo O, et al. Sox2 promotes tamoxifen resistance in breast cancer cells. *EMBO Mol Med*. 2014;6(1):66–79. doi:10.1002/emmm.201303411
70. Xu H, Tian Y, Yuan X, et al. Enrichment of CD44 in basal-type breast cancer correlates with EMT, cancer stem cell gene profile, and prognosis. *Onco Targets Ther*. 2016;9:431–444. doi:10.2147/OTT.S97192
71. Liu P, Kumar IS, Brown S, et al. Disulfiram targets cancer stem-like cells and reverses resistance and cross-resistance in acquired paclitaxel-resistant triple-negative breast cancer cells. *Br J Cancer*. 2013;109(7):1876–1885. doi:10.1038/bjc.2013.534
72. Matsuse H, Kohno S. Leukotriene receptor antagonists pranlukast and montelukast for treating asthma. *Expert Opin Pharmacother*. 2014;15(3):353–363. doi:10.1517/14656566.2014.872241
73. Nozaki M, Yoshikawa M, Ishitani K, et al. Cysteinyl leukotriene receptor antagonists inhibit tumor metastasis by inhibiting capillary permeability. *Keio J Med*. 2010;59(1):10–18. doi:10.2302/kjm.59.10
74. Sun T, Wu Z, Luo M, Lin D, Guo C. Pranlukast, a novel binding ligand of human Raf1 kinase inhibitory protein. *Biotechnol Lett*. 2016;38(8):1375–1380. doi:10.1007/s10529-016-2117-0
75. Escara-Wilke J, Yeung K, Keller ET. Raf kinase inhibitor protein (RKIP) in cancer. *Cancer Metastasis Rev*. 2012;31(3–4):615–620. doi:10.1007/s10555-012-9365-9